OPEN ACCESS
IOP Publishing
Journal of Physics: Condensed Matter
J. Phys.: Condens. Matter **37** (2025) 075001 (6pp)
https://doi.org/10.1088/1361-648X/ad9725

Band alignment at InP/TiO_2 interfaces from density-functional theory

Isaac Azahel Ruiz Alvarado[1,*], Christian Dreßler[2] and Wolf Gero Schmidt[1]

[1] Lehrstuhl für Theoretische Materialphysik, Universität Paderborn, 33095 Paderborn, Germany
[2] Insitut für Physik, TU Ilmenau, 98684 Ilmenau, Germany

E-mail: azahel.ruiz@uni-paderborn.de

Received 13 September 2024, revised 18 November 2024
Accepted for publication 25 November 2024
Published 5 December 2024

Abstract

The natural band alignments between indium phosphide and the main dioxides of titanium, i.e. rutile, anatase, and brookite as well as amorphous titania are calculated from the branch-point energies of the respective materials. Irrespective of the titania polymorph considered, type-I band alignment is predicted. This may change, however, in dependence on the microscopic interface structure: supercell calculations for amorphous titania grown on P-rich InP(001) surfaces result in a titania conduction band that nearly aligns with that of InP. Depending on the interface specifics, both type-I band and type-II band alignments are observed in the simulations. This agrees with recent experimental findings.

Keywords: interfaces, density functional theory, band alignment, InP, TiO_2, molecular dynamics

1. Introduction

Indium phosphide is frequently used in optoelectronics and high-speed electronics, see, e.g. [1, 2]. The InP band gap is close to the optimum for solar energy conversion [3]. Therefore, the material is also increasing used for photovoltaics [4] as well as in photoelectrochemical devices for water splitting [5]. In such devices, a thin TiO_2 film is often used as a corrosion protection layer [5–8]. The InP/TiO_2 heterojunction has also emerged as a promising candidate for solar cells [9] as well as for photocatalytic applications [10, 11].

While the structural and electronic properties of the InP growth plane are well understood [12–15], comparatively little is known about the InP/TiO_2 interface. This holds even for fundamental properties such as the interface band alignment. The band alignment, however, is crucial in determining how efficiently charge carriers (electrons and holes) move across the interface between the two materials. It will affect not only charge carrier flow and energy barriers, but also device efficiency and interface stability. Experimentally, it was found that TiO_2 serves as an effective hole blocking layer on the surface of InP while allowing the transport of electrons [16]. This would be consistent with a type-II junction. Yin *et al* [9], on the other hand, found the TiO_2 valence-band maximum (VBM) and conduction-band minimum (CBM) to be 2 eV below and 0.05 eV above the respective value of InP, corresponding to a type-I junction. Recently, Cipriano *et al* [17] used density-functional theory (DFT) to study microscopically the interface between the InP cleavage plane (110) with thin anatase TiO_2 films. Irrespective of the film thickness and irrespective of the TiO_2 surface orientation, a type-II band alignment was calculated, with the anatase CBM 0.10…0.64 eV below that of InP. This agrees with the experimental findings of [16], but does not necessarily contradict the measurements of Yin *et al* [9]:

* Author to whom any correspondence should be addressed.

Original Content from this work may be used under the terms of the Creative Commons Attribution 4.0 licence. Any further distribution of this work must maintain attribution to the author(s) and the title of the work, journal citation and DOI.

© 2024 The Author(s). Published by IOP Publishing Ltd

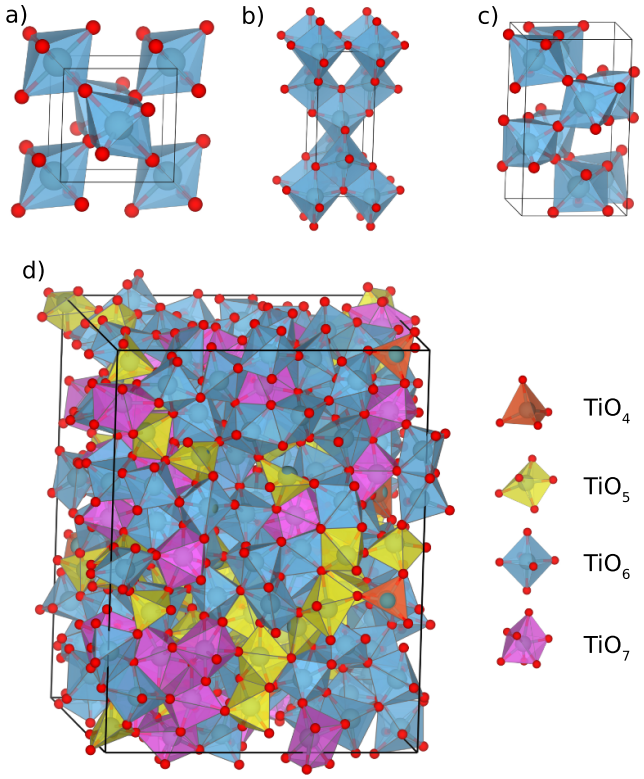

Figure 1. Polyhedra representation of the TiO_x building blocks used to model the (a) rutile, (b) anatase, and (c) brookite polymorphs of titania. An example structure of a-TiO_2 is shown in (d).

Anatase and rutile titania form a type-II interface, where the rutile CBM is 0.3…0.5 eV above the corresponding value of anatase [18–20]. As Yin *et al* employed atomic layer deposition (ALD) to deposit titania on InP, their measurements cannot directly be compared with calculations for anatase.

In order to better understand and to optimize the InP/TiO_2 interface, knowledge of the band alignment between the main dioxides of titanium, i.e. rutile, anatase, and brookite as well as amorphous titania (a-TiO_2) with indium phosphide is required. Corresponding data, based on DFT, are provided in the present work. On the one hand, the branch point energy (BPE) or charge neutrality level method [21–23] was used. The BPE method requires no knowledge of the structural details of the interface and provides accurate natural band alignments. On the other hand, the technologically particularly relevant case of an a-TiO_2 film deposited on P-rich InP(001):H—the InP surface typically obtained from gas phase epitaxy—is studied with microscopic supercell calculations.

2. Methodology

In the present work, the common crystalline titanium dioxide polymorphs rutile, anatase and brookite along with amorphous TiO_2 are studied, see figure 1. The atomic structures of the crystalline polymorphs are determined using DFT within the Vienna *ab-initio* Simulation Package (VASP) [24] implementation. Electron-ion interactions are described using the projector-augmented wave approach [25, 26]. In addition to the 3*d* and 4*s* states, also the 3*s* and 3*p* electrons are treated as valence states for Ti. Similarly, the In 4*d* states are considered in the valence shell, in addition to 5*s* and 5*p*. The PBE functional [27] within the general gradient approximation is used to calculate the exchange and correlation energy.

In order to generate atomic structures that model amorphous TiO_2, we start with classical molecular dynamics (MD) using the force field of Matsui and Akaogi [28] applied to a $4 \times 4 \times 8$ crystalline rutile supercell at 10 000 K. Subsequent to an 800 ps classical MD simulation run with the LAMMPS code [29], the structure was subjected to 10 ps *ab initio* MDs (AIMD) on the DFT level of theory using CP2K [30]. The AIMD was done using DZVP-MOLOPT-SR-GTH basis sets, Goedecker–Teter–Hutter pseudopotentials [31, 32] and the PBE functional [27] together with the empirical dispersion correction scheme (D3) of Grimme [33]. The temperature is set to 350 K applying a Nose–Hoover chain thermostat [34–36]. In order to obtain a representative ensemble of possible amorphous conformations, 10 equidistant snapshots were selected from the AIMD trajectory for detailed analysis of the electronic properties. The resulting amorphous bulk structures consist of 768 atoms in a tetragonal cell with lattice constants a = 18.4 and c = 23.67 Å. They are characterized by mostly 6-coordinated Ti ions with lesser amounts of 5 and 7-coordination and even fewer 4-coordinations. The average coordination number for Ti is 5.86, close to previous simulations [37, 38].

The InP/a-TiO_2 interface was modeled starting from the energetically favored InP(001)(2×2)2D–2H surface, the equilibrium surface structure resulting from gas-phase epitaxy [14, 15]. The InP slab consists of 12 layers. The bottom is passivated with partially charged pseudohydrogen ($Z = 1.25$). Computationally, the calculations are on the same footing as used in our previous InP(001) surface calculation, and well converged with respect to the numerical parameters [15, 39, 40]. A lateral (4×4) periodicity was chosen to allow for a realistic interface with a-TiO_2. The structure of the ∼18 Å thick amorphous titania overlayer containing 444 atoms was again obtained from MDs. Here, a protocol similar to the one described above for the preparation of bulk a-TiO_2 was used: Starting from the InP slab, additional TiO_2 building blocks were added to the simulation box, corresponding to the rutile structure. They were first subject to a classical MD at 2000 K—with the InP structure frozen - and subsequently thermalized using AIMD, as described above.

Natural band offsets of bulk materials can be obtained by aligning the branch point energies of the respective systems. Here the BPE are calculated following the formalism proposed, *inter alia*, by Schleife *et al* [41]. This approach has already successfully been applied to TiO_2 [18]. In detail, the BPE is obtained from

$$E_{\mathrm{BP}} \approx \frac{1}{2N_k} \sum_k \left[\frac{1}{N_{\mathrm{VB}}} \sum_i^{N_{\mathrm{VB}}} \varepsilon_{v_i} + \frac{1}{N_{\mathrm{CB}}} \sum_j^{N_{\mathrm{CB}}} \varepsilon_{c_j} \right], \qquad (1)$$

Table 1. Band gap energies calculated here in comparison to measured data.

Material		Band gap (eV) PBE	HSE06	Exp.
InP		0.44	1.40	1.34[a]
TiO_2	Rutile	1.82	3.32	3.3[b], 3.6[c]
	Anatase	2.09	3.59	3.8[d]
	Brookite	2.33	3.82	3.4[e]
	a-TiO_2	1.58	3.07[f]	

[a] Tian *et al* [46].
[b] Tezuka *et al* [47].
[c] Rangan *et al* [48].
[d] Wang *et al* [49].
[e] Koelsch *et al* [50].
[f] Extrapolated using the shift obtained for crystalline TiO_2.

where N_k is the total number of points used for Brillouin zone sampling and ε_{v_i} and ε_{c_j} are ith highest valence and jth lowest conduction band energies, respectively. The number of valence (N_{VB}) and conduction states (N_{CB}) that need to be included in equation (1) for converged results depends on the details of the band structure. For III–V compounds about two valence states and about one conduction state per two atoms (one of each species) is typically sufficient [41, 42]. Deak and co-workers used up to 12 valence and 10 conduction states per two TiO_2 units [18]. This approach has been followed here. Hybrid DFT using the HSE06 functional [43] as implemented in VASP [24] is used for an accurate description of the electronic structure, and in particular the band gap. The a-TiO_2 calculations involve averaging over AIMD snapshots obtained within a period between 0.25–4 ps. For the InP/a-TiO_2 interface the average was taken for an substantially longer period between 0.5–17 ps.

Deep core states were used in order to obtain the band offsets in the microscopic calculations for the InP(001)/a-TiO_2 interface. In detail, we used the 3*s* and 4*d* energies of Ti and In, respectively, to align the VBM in the respective bulk and supercell structures. Alternatively, a microscopic analysis can be performed based on the spatial projection of the electronic band structures, see, e.g. [44, 45].

3. Results and discussion

The fundamental bulk band gaps calculated here for the various materials are shown in table 1. The hybrid DFT results for InP and rutile as well as anatase compare well with experiment [46–49]. The apparently slightly larger deviations between experiment and theory for brookite may be related to the difficulties encountered to obtain it as a pure phase. In addition, it should be mentioned that the values derived in [49, 50] are based on optical measurements and will therefore be affected by excitonic effects [51].

The hybrid DFT band gap values in table 1 together with the hybrid BPE calculated from equation (1) are used to derive the natural band offsets. In case of a-TiO_2, the 768 atom supercell does for numerical reasons not allow for hybrid DFT calculations. However, given that both the band gap openings as well as the shifts of the BPE upon replacing PBE by HSE06 are essentially equal for all crystalline titania phases, we apply the same shifts to a-TiO_2. The natural band offsets thus calculated are summarized in table 2. Here, the valence band (ΔE_{VB}) and conduction band offsets (ΔE_{CB}) are referenced to InP bulk. The BPE values are consistent with previous studies for TiO_2 [18] and InP [52].

Table 2. Branch point energies and natural band offsets vs InP bulk for various TiO_2 phases calculated within hybrid DFT. All values in eV.

Material		BPE	ΔE_{VB}	ΔE_{CB}
InP		0.73		
TiO_2	Rutile	1.31	−0.59	1.34
	Anatase	1.82	−1.09	1.10
	Brookite	1.73	−1.00	1.43
	a-TiO_2[a]	1.19	−0.46	1.22

[a] Values extrapolated using the shifts obtained for crystalline TiO_2.

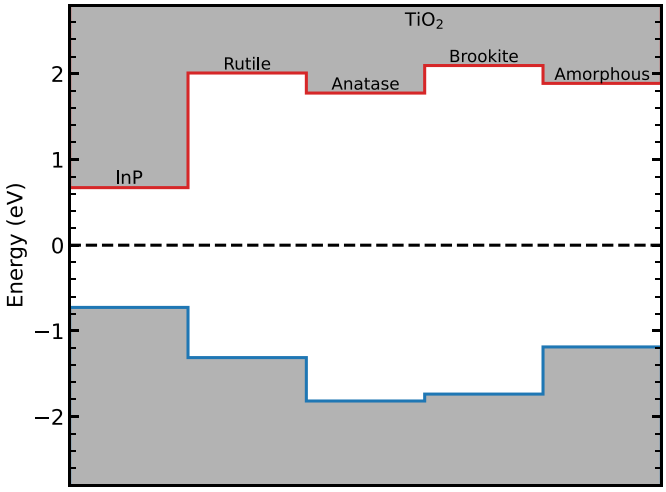

Figure 2. Natural band alignment between InP and various TiO_2 polymorphs calculated within hybrid DFT. The a-TiO_2 values are extrapolated.

The data from table 2 are visualized in figure 2, where the CBM and VBM are shown, all values are referenced to the BPE. The band gaps calculated for the various titania bulk phases considered here scatter within 0.7 eV. The scatter of the branch point energies is similar, around 0.6 eV. Nevertheless, all natural band offsets calculated are consistent with the type-I band alignment. This agrees with the data measured by Yin *et al* [9].

The natural band offsets calculated here are guidelines only for the actual band offsets, which will be affected by interface dipoles, interface strain as well as chemical bonding and stoichiometry changes at real interfaces. In order to see to what extent these effects will influence the interface band alignment, we perform microscopic calculations using DFT-PBE for one particularly relevant system, the interface between the

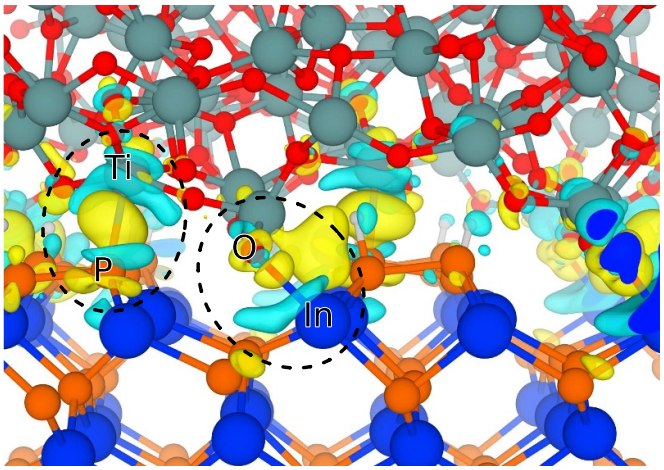

Figure 3. Atomic structure of the InP(001)/a-TiO_2 interface illustrating an example snapshot obtained from MD. Also shown is the charge density difference with respect to the separate bulk systems. Charge accumulation (depletion) is depicted in yellow (cyan). Examples of Ti–P and In–O bond formations are indicated.

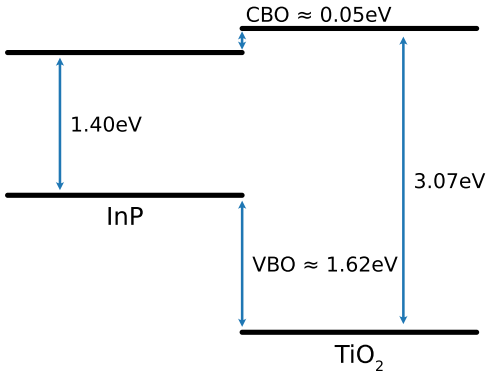

Figure 4. Band alignment of the InP(001)/a-TiO_2 interface calculated from the average of AIMD simulation snapshots. The In 4*d* and Ti 3*s* states were used to align the VBM of the InP and TiO_2, respectively.

P-rich InP(001) surface, i.e. the growth plane typically prepared using vapor phase epitaxy [40, 53, 54], and amorphous titania, as typically obtained from ALD [8, 55, 56]. For computational reasons, we cannot employ hybrid DFT to account for the quasiparticle energy corrections in all AIMD snapshot configurations. Rather, we use the extrapolation scheme applied earlier to a-TiO_2 bulk as presented in table 2. In order to evaluate the validity of this approximation, hybrid DFT calculations where performed for a single AIMD snapshot configuration. It was found that the extrapolation scheme agrees within an error bar of less than 0.2 eV with the hybrid DFT results.

An example AIMD snapshot of the interface is shown in figure 3. It can be seen that TiO_2 units occupy the trenches between the P dimer rows. The formation of In–O bonds with lengths in the range of 2.2–2.5 Å is observed from the calculated charge redistribution. Still, the essential features of the InP(001) surface remain intact. This agrees with the interpretation of recent x-ray and ultraviolet photoelectron spectroscopy data measured on titania films grown on InP(001) via ALD [8]. Cipriano *et al* [17] studied computationally the interface between InP and crystalline (anatase) titania. They observed the formation of In–O bonds and Ti–P bonds with lengths of about 2.3 and 2.7–2.8 Å, respectively. This is confirmed by the present simulations, where in addition to In–O bonds also Ti–P bonds are formed, see figure 3.

The AIMD interface snapshot configurations are used to calculate the interface band offsets microscopically. This is done by aligning the energies of the 3*s* and 4*d* energies of Ti and In in bulk structures with the respective values in the interface supercell. The average results are shown in figure 4. It can be seen that compared to the natural band alignment a substantial down shift of the titania band edges with respect to InP occurs. It amounts to 1.14 eV. Still, the calculated band alignment remains type-I. However, the conduction band offset is extremely small and in some AIMD snapshot configurations the alignment is type-II. This agrees with our calculations for the valence and conduction band offsets for the various realizations of a-TiO_2 with respect to InP bulk: The results obtained for the snapshot configurations are characterized by standard deviations of 0.28 and 0.23 eV for ΔE_{VB} and ΔE_{CB}, respectively. This is well above the conduction band band offset determined here microscopically for the InP(001)/a-TiO_2 interface. Obviously, the specific realization of the amorphous TiO_2 film in dependence on the actual preparation conditions [37, 38] will noticeable affect the band alignment. Both, type-I and type-II heterojunctions may occur for InP/a-TiO_2 interfaces. The present computational results are in accord with the experimental observations, where depending on the InP(001)/a-TiO_2 interface preparation type-II [8, 16] as well as type-I alignment [9] is found.

However, not only the properties of the amorphous titania film will affect the band alignment. It will also depend on the interface dipole [57]. Given that the InP(001) surface dipole varies by as much as one eV in dependence on the surface stoichiometry [39, 58], indeed a very wide range of band offsets can be realized.

4. Summary and conclusions

The present calculations predict natural band offsets corresponding to a type-I band alignment for InP/TiO_2 interfaces, irrespective of the titania polymorph. However, there is an appreciable scatter of the band offsets. The valence band offset is largest for anatase, −1.1 eV, and smallest for a-TiO_2, −0.5 eV. The conduction band offset varies between 1.1 eV for anatase and 1.4 eV for brookite. Even larger changes can be expected to result from the microscopic structure of the interface. In case of the technologically relevant interface between a-TiO_2 and P-rich InP(001), the calculations predict a valence band offset of −1.6 eV, while the conduction band offset is essentially quenched. Depending on the properties of

the amorphous titania film, both type-I and type-II interfaces can be realized. The results presented here thus demonstrate that by controlling the microscopic interface structure and the atomic order of the titania film a very wide range of band alignments becomes accessible.

Data availability statement

All data that support the findings of this study are included within the article (and any supplementary files).

Acknowledgments

The DFG (TRR 142/3-2024—Project Numbers 231447078 and SCHM1361/33) is greatfully acknowledged for financial support. We thank the Paderborn Center for Parallel Computing (PC^2) and the Höchstleistungs-Rechenzentrum Stuttgart (HLRS) for grants of high-performance computer time.

Conflict of interest

The authors declare no conflict of interest.

ORCID iDs

Isaac Azahel Ruiz Alvarado https://orcid.org/0000-0002-4710-1170
Christian Dreßler https://orcid.org/0000-0002-0145-1263
Wolf Gero Schmidt https://orcid.org/0000-0002-2717-5076

References

[1] Yan Z, Han Y, Lin L, Xue Y, Ma C, Ng W K, Wong K S and Lau K M 2021 A monolithic InP/SOI platform for integrated photonics *Light Sci. Appl.* **10** 200
[2] Mukherjee C *et al* 2021 Towards monolithic indium phosphide (InP)-based electronic photonic technologies for beyond 5G communication systems *Appl. Sci.* **11** 2393
[3] Loferski J J 1956 Theoretical considerations governing the choice of the optimum semiconductor for photovoltaic solar energy conversion *J. Appl. Phys.* **27** 777
[4] Raj V, dos Santos T S, Rougieux F, Vora K, Lysevych M, Fu L, Mokkapati S, Tan H H and Jagadish C 2018 Indium phosphide based solar cell using ultra-thin ZnO as an electron selective layer *J. Phys. D: Appl. Phys.* **51** 395301
[5] Gao L *et al* 2016 High-efficiency InP-based photocathode for hydrogen production by interface energetics design and photon management *Adv. Funct. Mater.* **26** 679
[6] Cheng W-H, Richter M H, May M M, Ohlmann J, Lackner D, Dimroth F, Hannappel T, Atwater H A and Lewerenz H-J 2018 Monolithic photoelectrochemical device for direct water splitting with 19% efficiency *ACS Energy Lett.* **3** 1795
[7] Hannappel T *et al* 2024 Integration of multijunction absorbers and catalysts for efficient solar-driven artificial leaf structures: a physical and materials science perspective *Sol. RRL* **8** 2301047
[8] Diederich J *et al* 2024 Ultrafast electron dynamics at the p-rich indium phosphide/TiO_2 interface *Adv. Funct. Mater.* 2409455
[9] Yin X, Battaglia C, Lin Y, Chen K, Hettick M, Zheng M, Chen C-Y, Kiriya D and Javey A 2014 19.2% efficient InP heterojunction solar cell with electron-selective TiO_2 contact *ACS Photonics* **1** 1245
[10] Qiu J, Zeng G, Ha M-A, Ge M, Lin Y, Hettick M, Hou B, Alexandrova A N, Javey A and Cronin S B 2015 Artificial photosynthesis on TiO_2-passivated InP nanopillars *Nano Lett.* **15** 6177
[11] Zeng G, Qiu J, Hou B, Shi H, Lin Y, Hettick M, Javey A and Cronin S B 2015 Enhanced photocatalytic reduction of CO_2 to CO through TiO_2 passivation of InP in ionic liquids *Chem. Eur. J.* **21** 13502
[12] Schmidt W G 1997 (4×2) and (2×4) reconstructions of GaAs and InP(001) surfaces *Appl. Phys.* A **65** 581
[13] Schmidt W G 2002 III–V compound semiconductor (001) surfaces *Appl. Phys.* A **75** 89
[14] Schmidt W G, Hahn P H, Bechstedt F, Esser N, Vogt P, Wange A and Richter W 2003 InP(001)-(2×1) surface: a hydrogen stabilized structure *Phys. Rev. Lett.* **90** 126101
[15] Sciotto R, Ruiz Alvarado I A and Schmidt W G 2024 Substrate doping and defect influence on P-rich InP(001):H surface properties *Surfaces* **7** 79
[16] Lin Y *et al* 2015 Role of TiO_2 surface passivation on improving the performance of p-InP photocathodes *J. Phys. Chem.* C **119** 2308
[17] Cipriano L A, Di Liberto G, Tosoni S and Pacchioni G 2021 Structure and band alignment of InP photocatalysts passivated by TiO_2 thin films *J. Phys. Chem.* C **125** 11620
[18] Deák P, Aradi B and Frauenheim T 2011 Band lineup and charge carrier separation in mixed rutile-anatase systems *J. Phys. Chem.* C **115** 3443
[19] Scanlon D O *et al* 2013 Band alignment of rutile and anatase TiO_2 *Nat. Mater.* **12** 798
[20] Pfeifer V *et al* 2013 Energy band alignment between anatase and rutile TiO_2 *J. Phys. Chem. Lett.* **4** 4182
[21] Tersoff J 1984 Theory of semiconductor heterojunctions: the role of quantum dipoles *Phys. Rev.* B **30** 4874
[22] Flores F and Tejedor C 1979 Energy barriers and interface states at heterojunctions *J. Phys. C: Solid State Phys.* **12** 731
[23] van de Walle C G and Neugebauer J 2003 Universal alignment of hydrogen levels in semiconductors, insulators and solutions *Nature* **423** 626
[24] Kresse G and Furthmüller J 1996 Efficiency of ab-initio total energy calculations for metals and semiconductors using a plane-wave basis set *Comput. Mater. Sci.* **6** 15
[25] Blöchl P E 1994 Projector augmented-wave method *Phys. Rev.* B **50** 17953
[26] Kresse G and Joubert D 1999 From ultrasoft pseudopotentials to the projector augmented-wave method *Phys. Rev.* B **59** 1758
[27] Perdew J P, Burke K and Ernzerhof M 1996 Generalized gradient approximation made simple *Phys. Rev. Lett.* **77** 3865
[28] Matsui M and Akaogi M 1991 Molecular dynamics simulation of the structural and physical properties of the four polymorphs of TiO_2 *Mol. Simul.* **6** 239
[29] Thompson A P *et al* 2022 LAMMPS—a flexible simulation tool for particle-based materials modeling at the atomic, meso and continuum scales *Comput. Phys. Commun.* **271** 108171
[30] Kühne T D *et al* 2020 CP2K: an electronic structure and molecular dynamics software package—QUICKSTEP:

efficient and accurate electronic structure calculations *J. Chem. Phys.* **152** 194103
[31] Hartwigsen C, Goedecker S and Hutter J 1998 Relativistic separable dual-space Gaussian pseudopotentials from H to Rn *Phys. Rev.* B **58** 3641
[32] Krack M 2005 Pseudopotentials for H to Kr optimized for gradient-corrected exchange-correlation functionals *Theor. Chem. Acc.* **114** 145
[33] Grimme S, Antony J, Ehrlich S and Krieg H 2010 A consistent and accurate ab initio parametrization of density functional dispersion correction (DFT-D) for the 94 elements H-Pu *J. Chem. Phys.* **132** 154104
[34] Nosé S 1984 A unified formulation of the constant temperature molecular dynamics methods *J. Chem. Phys.* **81** 511
[35] Martyna G J, Klein M L and Tuckerman M 1992 Nosé–Hoover chains: the canonical ensemble via continuous dynamics *J. Chem. Phys.* **97** 2635
[36] Nosé S 1984 A molecular dynamics method for simulations in the canonical ensemble *Mol. Phys.* **52** 255
[37] Landmann M, Köhler T, Köppen S, Rauls E, Frauenheim T and Schmidt W G 2012 Fingerprints of order and disorder in the electronic and optical properties of crystalline and amorphous TiO_2 *Phys. Rev.* B **86** 064201
[38] Landmann M, Köhler T, Rauls E, Frauenheim T and Schmidt W G 2014 The atomic structure of ternary amorphous $Ti_xSi_{1-x}O_2$ hybrid oxides *J. Phys.: Condens. Matter* **26** 253201
[39] Ruiz Alvarado I A and Schmidt W G 2022 Water/InP(001) from density functional theory *ACS Omega* **7** 19355
[40] Moritz D, Alvarado I R, Pour M Z, Paszuk A, Frieß T, Runge E, Hofmann J, Hannappel T, Schmidt W G and Jaegermann W 2022 P-terminated InP(001) surfaces: surface band bending and reactivity to water *ACS Appl. Mater. Interfaces* **14** 47255
[41] Schleife A, Fuchs F, Rödl C, Furthmüller J and Bechstedt F 2009 Branch-point energies and band discontinuities of III-nitrides and III-/II-oxides from quasiparticle band-structure calculations *Appl. Phys. Lett.* **94** 012104
[42] Meier L, Braun C, Hannappel T and Schmidt W G 2021 Band alignment at $Ga_xIn_{1-x}P/Al_yIn_{1-y}P$ alloy interfaces from hybrid density functional theory calculations *Phys. Status Solidi* b **258** 2000463
[43] Krukau A V, Vydrov O A, Izmaylov A F and Scuseria G E 2006 Influence of the exchange screening parameter on the performance of screened hybrid functionals *J. Chem. Phys.* **125** 224106
[44] Zhou B, Gong S-J, Jiang K, Xu L, Zhu L, Shang L, Li Y, Hu Z and Chu J 2019 Ferroelectric and dipole control of band alignment in the two dimensional InTe/In_2Se_3 heterostructure *J. Phys.: Condens. Matter* **32** 055703
[45] Zhou B, Jiang K, Shang L, Zhang J, Li Y, Zhu L, Gong S-J, Hu Z and Chu J 2020 Enhanced carrier separation in ferroelectric In_2Se_3/MoS_2 van der Waals heterostructure *J. Mater. Chem.* C **8** 11160
[46] Tian S *et al* 2014 Surface state and optical property of sulfur passivated InP *Mater. Sci. Semicond. Process.* **17** 33
[47] Tezuka Y, Shin S, Ishii T, Ejima T, Suzuki S and Sato S 1994 Photoemission and bremsstrahlung isochromat spectroscopy studies of TiO_2 (rutile) and $SrTiO_3$ *J. Phys. Soc. Japan* **63** 347
[48] Rangan S, Katalinic S, Thorpe R, Bartynski R A, Rochford J and Galoppini E 2010 Energy level alignment of a Zinc(II) tetraphenylporphyrin dye adsorbed onto TiO_2(110) and ZnO($11\bar{2}0$) surfaces *J. Phys. Chem.* C **114** 1139
[49] Wang Z, Helmersson U and Käll P-O 2002 Optical properties of anatase TiO_2 thin films prepared by aqueous sol–gel process at low temperature *Thin Solid Films* **405** 50
[50] Koelsch M, Cassaignon S, Guillemoles J and Jolivet J 2002 Comparison of optical and electrochemical properties of anatase and brookite TiO_2 synthesized by the sol–gel method *Thin Solid Films* **403–404** 312
[51] Landmann M, Rauls E and Schmidt W G 2012 The electronic structure and optical response of rutile, anatase and brookite TiO_2 *J. Phys.: Condens. Matter* **24** 195503
[52] Shapera E P and Schleife A 2018 Database-driven materials selection for semiconductor heterojunction design *Adv. Theory Simul.* **1** 1800075
[53] Vogt P, Frisch A, Hannappel T, Visbeck S, Willig F, Jung C, Follath R, Braun W, Richter W and Esser N 2000 Atomic structure and composition of the P-rich InP(001) surfaces *Appl. Surf. Sci.* **166** 190
[54] Diederich J *et al* 2024 Unraveling electron dynamics in p-type indium phosphide (100): a time-resolved two-photon photoemission study *J. Am. Chem. Soc.* **146** 8949
[55] Lee M H *et al* 2012 p-type InP nanopillar photocathodes for efficient solar-driven hydrogen production *Angew. Chem., Int. Ed.* **51** 10760
[56] Hu S, Richter M H, Lichterman M F, Beardslee J, Mayer T, Brunschwig B S and Lewis N S 2016 Electrical, photoelectrochemical and photoelectron spectroscopic investigation of the interfacial transport and energetics of amorphous TiO_2/Si heterojunctions *J. Phys. Chem.* C **120** 3117
[57] Yajima T, Hikita Y, Minohara M, Bell C, Mundy J A, Kourkoutis L F, Muller D A, Kumigashira H, Oshima M and Hwang H Y 2015 Controlling band alignments by artificial interface dipoles at perovskite heterointerfaces *Nat. Commun.* **6** 6759
[58] Schmidt W and Bechstedt F 1998 Geometry and electronic structure of InP(001)(2×4) reconstructions *Surf. Sci.* **409** 474